

The use of CVD-diamond for heavy-ion detection

E. Berdermann^{*,1}, K. Blasche, P. Moritz, H. Stelzer¹, B. Voss

Gesellschaft für Schwerionenforschung, Planckstraße 1, 64291 Darmstadt, Germany

Abstract

The suitability of CVD-diamond detectors is investigated for applications in heavy-ion accelerator facilities with high intensity beams. Various diamond films of ‘optical’ and ‘electronic grade’ used and unpolished (as grown) are tested with different ions from α -particles (^{241}Am -source) up to the heaviest ions like ^{208}Pb and ^{238}U . The diamond signals are processed in a single-particle mode with current sensitive low-noise broadband electronics. An intrinsic time resolution of $\sigma_t(\Delta T) = 29$ ps is achieved using detectors of ‘optical grade’ with a thickness of 100 μm . The time resolution improves for thicker samples and for higher electric field applied to the detector. Determined by the strip capacitance and the electronics used, a single-particle counting rate capability $> 10^8$ ions/s is obtained. The charge collected from different particles increases linearly with the energy loss of the particle and non-linearly with the detector thickness. The pulse-height resolution depends strongly on the material texture and on the irradiation state of the sample and weakly on the ionisation density produced by the particle. ‘Priming’ is observed up to a fluence of 10^{10} ions/ cm^2 . The homogeneity over the detector area increases significantly. The charge-collection efficiency improves by a factor of 2 and the pulse-height resolution significantly by a factor of 5. The bandwidth of available electronics limits the results obtained at present. Nevertheless, the selection of data presented demonstrates an excellent suitability of CVD diamond for a variety of heavy-ion applications. © 2001 Elsevier Science B.V. All rights reserved.

Keywords: CVD diamond; Heavy-ion timing detectors; Single-particle processing

1. Introduction

Depending on the energy and mass of the projectile and target the multiplicity of one event in fixed-target nuclear physics experiments can vary from 2 (elastic reaction) up to > 2000 created particles. The event constituents are heavy particles emitted from projectile- and target nuclei down to singly-charged protons, electrons, pions and kaons as well as high energy photons and neutrons.

An overview of various detector devices applied in nuclear-physics experiments at present is given in Ref. [1]. Heavy ions (HI) are identified by the determination of their mass A , their nuclear charge Z and their

charge state q , which reduces Z to an effective value Z_{eff} . When radiative energy loss is negligible the total energy loss ΔE of a traversing HI in matter is stated in terms of dE/dx given by the simplified Bethe–Bloch relation Eq. (1):

$$-\frac{dE}{dx} \propto \frac{Z_{\text{eff}}^2}{\beta^2} \cdot \left[\ln \frac{2m_e c^2 \beta^2}{I \cdot (1 - \beta^2)} - \beta^2 \right] \quad \text{with } \beta = \frac{v}{c} \quad (1)$$

where Z_{eff} and v are the effective charge and the velocity of the particle, m_e the electron mass and I the mean excitation energy of the target atoms. The dynamic range of the total energy loss ΔE in one event can be 1:10 000.

ΔE does not depend on the mass A of the impinging particle. Magnetic analysis is used to determine the mass A and the charge state q of the ion and Time of Flight (ToF) measurements are performed to define v . In order to obtain reaction cross-sections the precise

* Corresponding author.

E-mail address: e.berdermann@gsi.de (E. Berdermann).

¹Members of the RD42 Collaboration.

number of the produced particles as well as the absolute beam intensity have to be known. Time-zero detectors select projectiles undergoing reactions with target nuclei $1/10^9$ ions/spill.

The recently installed high-current injector of the HI accelerator facilities at GSI delivers ion beams with an intensity of 10^{11} ions/spill. In the case of beam diagnostics no detector used at present [2] provides absolute particle monitoring under such HI bombardment. The radiation resistance found for CVD diamond [3–5] initiated a development of diamond detectors capable to operate at particle rates above 10^9 ions/s [6]. The presence of electrical defects reducing the charge-collection efficiency (CCE) of diamond detectors [7] is tolerable considering the high amount of charge produced by heavy charged particles in solid state detectors.

The way to use CVD diamond for a significant improvement of HI measurements is the subject of this report. The fast diamond response processed with low noise broadband electronics [8] provides signals with a rise time < 300 ps and a pulse width ≈ 1 ns. These characteristics lead to both a good ToF resolution and a high single-particle counting rate capability. Applications in atomic and nuclear physics as well as in accelerator beam diagnostics and in the tumor therapy with carbon ions at GSI are developed and a short overview of the devices is given in Section 4.

2. Preparation of HI diamond detectors

2.1. Detector setup

The setup principle is demonstrated in Fig. 1. The diamond films are glued on ceramic boards mounted in light tight r.f.-sealed aluminum boxes. Each diamond

channel is built up as a 50- Ω microstrip transmission line. The nucleation side usually at zero potential (left) is connected with broad brass springs to the fully metallized back side of the ceramics. The growth side is band or wire bonded to an r.f. suitable coaxial connector (right). The stripline provides both the high voltage supply and the detector input to the amplifier. The advantage of such a design is a stable pick-up free operation. Moreover, due to a larger distance between detector and amplifier, no radiation hard electronics are needed.

2.2. Signal processing

The high band gap of 5.5 eV avoids the need for a pn-junction. Diamond detectors are biased positively or negatively. A traversing charged particle produces excess electron hole pairs (e-h) in the diamond bulk. Charge traps inhomogeneously distributed inside the diamond produce local fields modifying the homogeneous electric field applied [9]. The (e-h) separate and drift to the electrodes guided by the local average electric field. Assuming a material with very low concentration of traps the saturated drift velocity is $200 \mu\text{m/ns}$ [4]. Since the average drift time in unpolished CVD diamond is < 1 ns a low-noise current-sensitive broadband amplifier DBA-II (Diamond Broadband Amplifier, 2 GHz) [8] is used to amplify the induced current signal $I_g(t)$.

The simple relations describing the detector response to a traversing charged particle are given in Eqs. (2) and (3):

$$\frac{dQ_g}{dt} = I_g(t); I_c(t) = I_g(t) \cdot e^{-t/RC_D} \quad (2)$$

whereas $Q_g(t), I_g(t)$ are the charge and corresponding current generated, $I_c(t)$ the collected current during

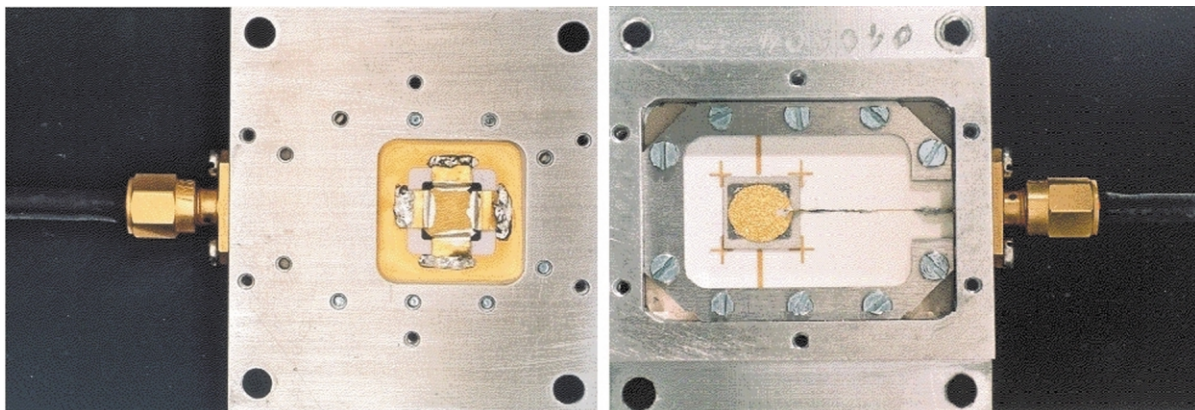


Fig. 1. Each single-channel of a CVD-diamond HI detector is connected via a 50- Ω microstrip line to the amplifier. The fully metallized backside of the ceramic pcb at ground potential is connected to the nucleation side (left) and the growth side (right) to an r.f. suitable coaxial connector (SMA).

$0 \leq t \leq \tau$ which is the drift time of the charge carriers, R the impedance of the amplifier used and C_D the detector capacitance.

The collected charge Q_c is obtained from the corresponding amplifier input pulse $U_c(t) = I_c(t) \cdot R$:

$$Q_c(t) = \frac{1}{R} \int_0^\tau U_c(t) \cdot dt \quad (3)$$

The bandwidth of the DBA-II amplifier used at present is 2 GHz and the gain is fixed at 100. A new design with variable gain is currently under development. The amplified signals are further processed with commercially available nuclear electronics. Fig. 2 shows a circuit used for ToF and in-beam pulse-height measurements (Section 3).

2.3. Detector characterisation

Leakage current (I_D) does not affect the detector performance if AC-coupled amplifiers are used. In order to check the metallic contacts and to ensure a stable operation $I_D(E_D)$ characteristics are measured [3–6] whereas E_D is the electric field applied to the detector. The most important parameters classifying HI diamond detectors are the rise (t_r) and the decay (t_d) time of the single-particle pulses. Fig. 3 shows characterisation data of a sample with an area of $1 \times 1 \text{ cm}^2$, a thickness of $d_D = 93 \text{ }\mu\text{m}$ and a capacitance of $C_D = 37.2 \text{ pF}$. ^{84}Kr ions of 650 MeV/amu are used. The single pulses (Fig. 3a) correspond to an energy loss ΔE of 97.3 MeV . A histogram plot is chosen in order to indicate the sampling of the broadband oscilloscope used for analysis. The improvement of Q_c when increasing the bias is shown in (Fig. 3c) and collected charge distributions at $E = \pm 1 \text{ V/}\mu\text{m}$ in (Fig. 3d).

The ^{84}Kr single shots selected randomly for presentation demonstrate the limitation of the measurement system to determine the signal rise time. Although the

mean values of the decay time distributions t_d (Fig. 3b) are dominated by the RC_D constant, a shorter carrier drift time is indicated at negative polarity. However, the quality of a HI diamond detector is characterized by the widths of those distributions. The dispersion of t_D mirrors the variety of traps appearing in the diamond bulk and thus the width of the Q_C spectra shown in (Fig. 3d). The uniform rise time is exploited for ToF measurements and the narrow FWHM for high-rate counting.

3. Experimental results

3.1. Irradiation tests

The maximum HI fluence which can be used without damaging CVD diamond is still unknown. No degradation of the diamond pulse heights and no increase in the leakage current was observed after an irradiation with $5 \times 10^{10}/\text{cm}^2$ traversing ^{238}U ions of 1 GeV/amu [6]. The energy loss in this case is 1 GeV/ion . This lower limit for radiation hardness is confirmed by measurements with ^{12}C ions of 5.9 MeV/amu stopped in the diamond bulk. Each ^{12}C ion deposits 70 MeV at Bragg–Maximum, which is a thin layer at $53 \text{ }\mu\text{m}$ depth. After irradiation with 10^{10} carbon ions/ cm^2 the homogeneity of the sample was improved such that the flat exponential slope obtained at 10^8 ions/ cm^2 was changed to a Gaussian with a clear separation from the electronic noise. This in heavy-ion measurements hitherto unobserved ‘priming’ [3,5,7,9] effect is illustrated impressively in Fig. 4. CCE distributions are shown at a fluence of 10^8 ions/ cm^2 (a) and at a fluence of 10^{10} ions/ cm^2 (b), respectively [10]. The average collected charge improves from 28 to 54% and the pulse-height resolution FWHM/MP (most probable) from 5.2 to 1.04, respectively.

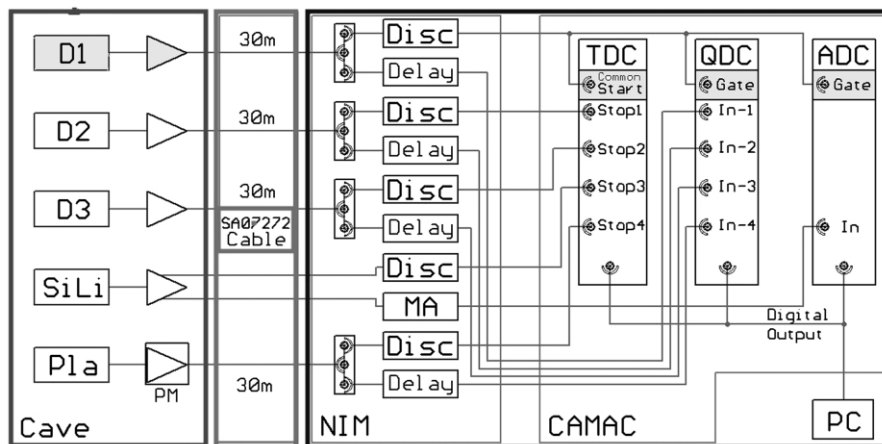


Fig. 2. Schematics of the electronic circuit used for ToF and in-beam pulse-height measurements. A silicon detector (Sili) and a plastic scintillator (Pla) are used in coincidence.

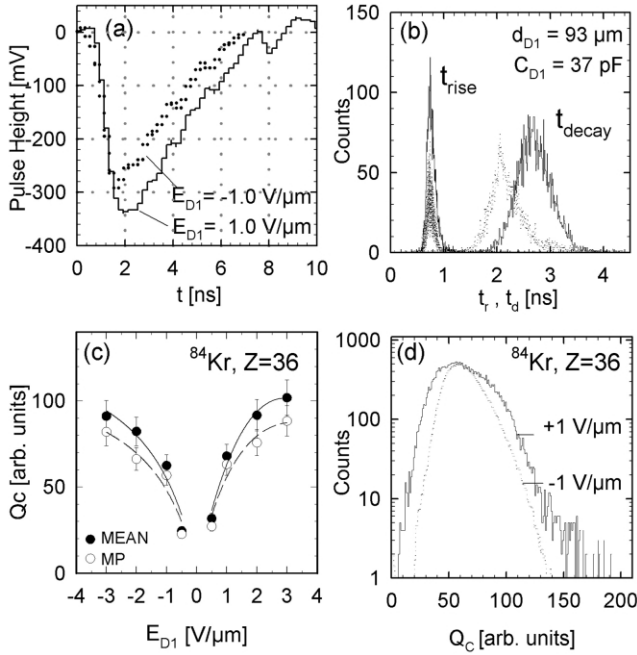


Fig. 3. Characterisation data of a HI CVD-diamond detector. (a) Single-particle pulses. (b) Rise and decay time distributions. (c) Electric field dependence of the collected charge Q_c . (d) Collected charge distributions. The data are limited due to the bandwidth of today's electronics.

3.2. Counting rate capability and time resolution

The single-particle count rate measured with a diamond detector of an area of $1 \times 1 \text{ cm}^2$ and a capacitance of $C_D = 9 \text{ pF}$ was compared to the beam intensity monitored with an ionisation chamber (IC, current integration mode). Both rates measured in an external beam transport are plotted in Fig. 5a vs. the total number of ions as measured with a beam-current transformer inside a synchrotron ring. Due to a beam size larger than the active detector area a lower rate compared to the IC rate is obtained. However, the lower limit of $3 \times 10^8 \text{ ions/s}$ measured for one diamond

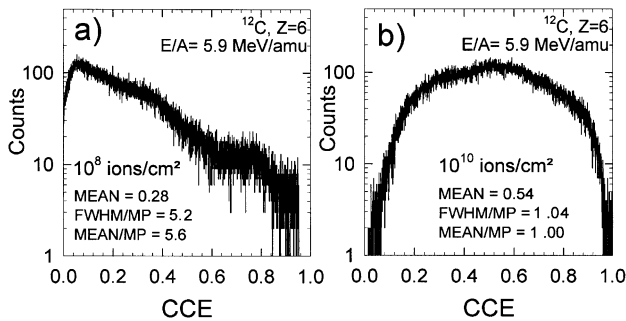


Fig. 4. Charge collection efficiency (CCE) distributions measured with ^{12}C ions of 5.9 MeV/amu stopped in the diamond bulk. (a) At a fluence of 10^8 ions/cm^2 (b) at a fluence of $10^{10} \text{ ions/cm}^2$. ‘Priming’ increases the CCE by a factor of 2 and the FWHM/MP by a factor of 5.

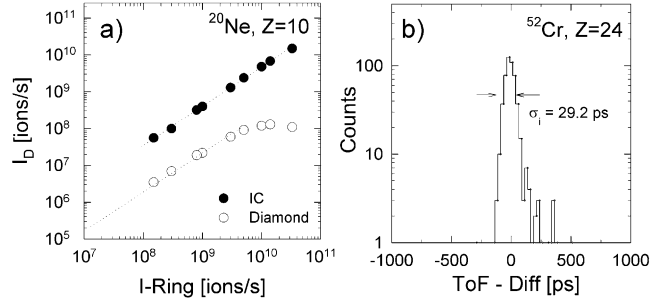


Fig. 5. (a) The beam intensity measured with a diamond detector (open circles, single-particle mode) and with an ionisation chamber (IC, black dots, current mode) in an external beamline plotted over the current measured inside a synchrotron with beam current transformers. The constant deviation from the IC rate is due to a beam size larger than the diamond sample. The 500-MHz scaler used limit the diamond rate beyond 10^8 ions/s . (b) ToF resolution obtained with ^{52}Cr ions and two detectors of ‘optical grade’ and a thickness of $100 \mu\text{m}$. The intrinsic resolution is $\sigma_i = \sigma/\sqrt{2} = 29 \text{ ps}$.

channel is given by the 500-MHz scaler used. It is expected that the count rate capability of a large area detector divided in several strips should be approximately 10^{10} ions/s .

An intrinsic time resolution of $\sigma_i = 29 \text{ ps}$ is achieved with ^{52}Cr ions of 650 MeV/amu using the start-veto device of the HADES [12] spectrometer. The two diamond octagons of ‘optical grade’ have a thickness of $100 \mu\text{m}$ and a strip capacitance of 8.3 pF. The narrow Gaussian distribution obtained is shown in Fig. 5b.

3.3. Pulse-height resolution

3.3.1. The dependence on the CVD diamond texture

Comparing the ^{58}Ni fragmentation spectrum measured with a polycrystalline CVD-diamond detector (Fig. 6a) to that obtained simultaneously from a single-crystal silicon detector (Fig. 6b) a dependence of the pulse-height resolution on the material texture is suggested. No individual fragments are discriminated in the case of the polycrystalline diamond detector.

Many detailed investigations of CVD diamond using

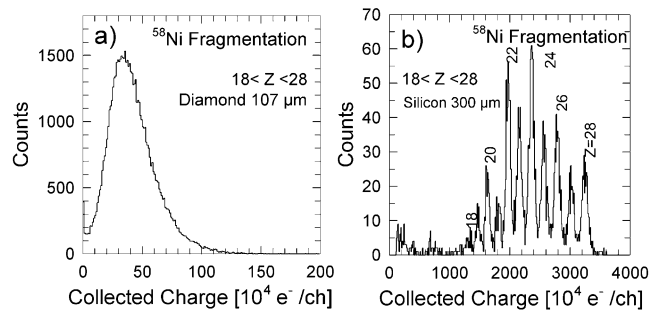


Fig. 6. ^{58}Ni fragmentation spectrum measured with a CVD diamond detector (a) and with a single-crystal silicon detector (b) in the same experiment. No individual fragments are discriminated by the polycrystalline diamond detector.

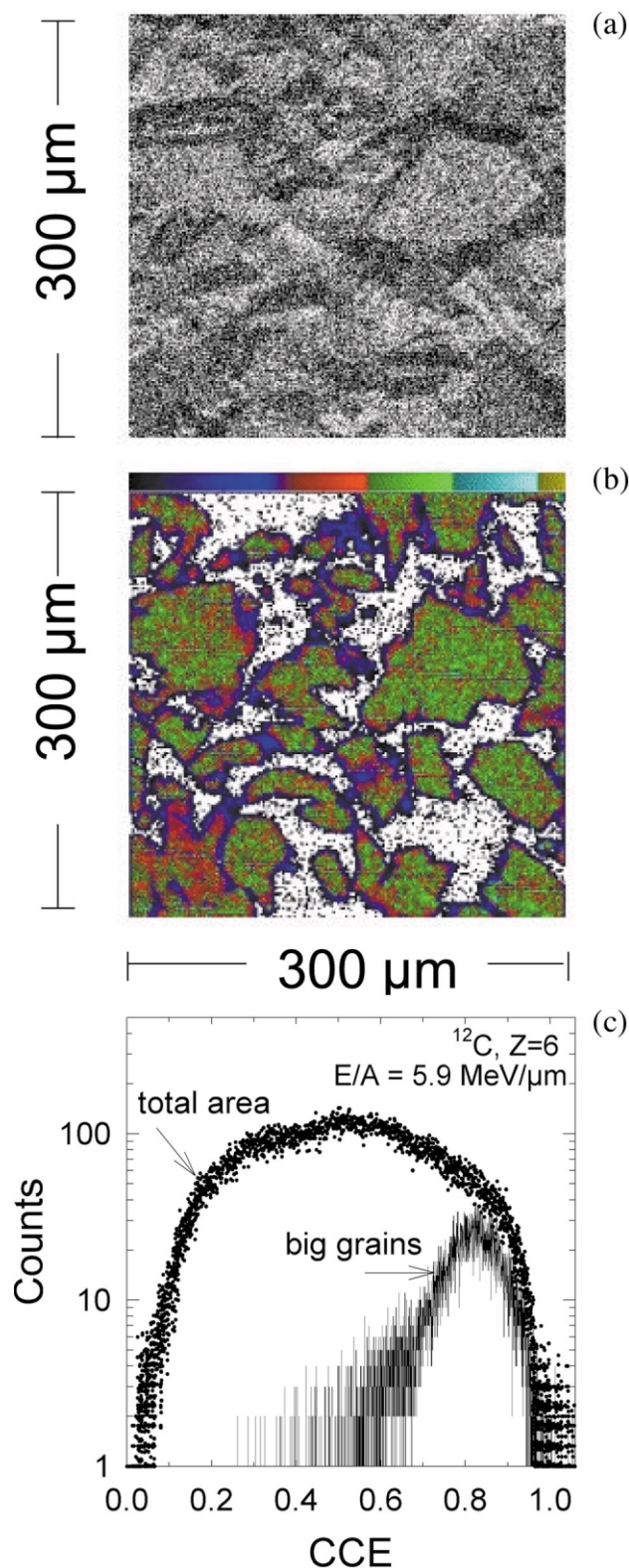


Fig. 7. (a) Surface topology of the irradiated growth side area of $300 \times 300 \mu\text{m}^2$. (b) The corresponding CCE map. The colour ID (palette on top) indicates increasing values from the left to the right. White colour is zero counts. (c) The CCE distributions obtained from the total area (dotted lines) and from the big grains (full line) visible on the surface. The highest amount of charge is collected from these grains.

proton microbeams have been reported [9,13]. With the HI microprobe facility at GSI, ^{12}C ions of 5.9 MeV/amu were implanted homogeneously in a diamond sample of a thickness of 390 μm. The irradiation was performed from the growth side [10]. The area scanned was $300 \times 300 \mu\text{m}^2$ and the range of the ions was 57 μm. In Fig. 7(a) the secondary electron emission spectrum (SEM) obtained simultaneously from the irradiated surface is shown. The corresponding CCE distribution of the total scanned area (dotted lines) is overlaid in Fig. 7(c) to the distribution from selected big-grains visible on the surface. Although the nature of the grains is unknown the significantly improved resolution obtained indicates a single-crystal structure or a dependence of the resolution on the grain size. In agreement to that the CCE map (Fig. 7(b)) shows the highest amount of charge collected from these grains.

3.3.2. The dependence on the ionisation density

In Fig. 8 the charge collected from individual ^{58}Ni fragments selected by a magnetic system and identified with a high-resolution MUSIC chamber (Multiple Sampling Ionisation Chamber) are plotted over the Z^2 of the corresponding ion. All fragments are emitted with projectile velocity. The diamond signals are calibrated with a silicon detector. Charge-sensitive amplifiers are used in this case. Despite the huge amount of charge loss the MEAN Q_C (a) increases proportional to the energy loss whereas the MP values show a constant deviation of 15%. The solid line indicates the theoretical values multiplied by 0.1, which is the CCE of this sample.

The MP/NOISE ratio increases by a factor of 2.4 (b). Nevertheless, the resolution FWHM/MP remains within the error bars constant at 0.7 as well as the homogeneity ratio MEAN/MP at 1.2. Concluding, no significant dependence of the pulse-height resolution

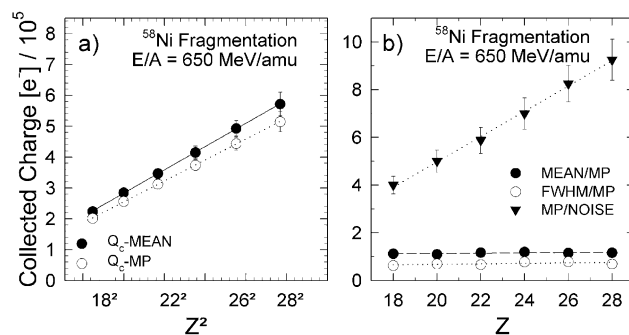


Fig. 8. ^{58}Ni fragmentation data measured with a diamond detector with a thickness of 107 μm at an electric field $E_D = -2.8 \text{ V}/\mu\text{m}$. (a) The MEAN values (squares) increase proportional to the energy loss (full line) whereas the MP values (dots) show a constant deviation of 15%. (b) Although the MP/N (triangles) increases by a factor of 2.4 the homogeneity ratio (MEAN/MP, black dots) and the pulse-height resolution (FWHM/MP, open circles) remain constant at 1.2 and at 0.7, respectively.

on the ionisation density is found within the range $18 \leq Z \leq 28$ analyzed.

3.4. Linearity

The dependence of the detector properties on the detector thickness was recently investigated systematically with ^{84}Kr ions of 650 MeV/amu. A preliminary analysis of the data is presented. Three detectors made of CVD diamond ‘electronic grade’, all of them grown at the same process parameters [14] were used. The samples were mounted in a stack with thickness increasing in beam direction ($d_{D1} = 93 \mu\text{m}$, $d_{D2} = 158 \mu\text{m}$, $d_{D3} = 246 \mu\text{m}$). The circuit used for the measurements is shown in Fig. 2. The first diamond detector in beam direction (D1) provides the common start for the ToF measurements with a Philips TDC (25 ps/ch) as well as the gates for the LeCroy QDC and an ORTEC ADC used for the silicon pulse-height measurements.

3.4.1. Collected charge distributions

The mean collected charge Q_C is found to be higher for positive bias (Fig. 9a) in contrary to the pulse-height resolution FWHM/MP (Fig. 9b). Q_C increases approximately linear for thin detectors and becomes significantly higher above a $d_D \approx 170 \mu\text{m}$. This trend is in agreement with the expectation of improving electrical properties along the crystal growth [3–5,9]. In Fig. 9c the ratio of the charge collected from two detectors is plotted over the corresponding ratio of the detector thickness. Data on the dotted line indicate a linear increase of Q_C with the detector thickness.

3.4.2. Time spectra

Krypton ToF spectra measured at negative resp. positive polarity are plotted in Fig. 10a. The σ -widths of the ToF distributions measured with D1 and D2 (ΔT_{12}), D1 and D3 (ΔT_{13}) as well as D2 and D3 (ΔT_{23}) are plotted in (b) over the electric field applied to the detectors. $\sigma(\Delta T)$ improves with increasing detector thickness as well as at higher electric field. $\sigma(\Delta T)$ saturates above an $E_D \approx \pm 2 \text{ V}/\mu\text{m}$.

4. Applications of diamond detectors for heavy ion beams [11]

Samples of different size and shape are used. Octagonal shaped detectors matching the local beam profile are designed as well as squares with strip or pixel electrodes with a pitch on the order of millimeters. The largest diamond detector of a $60 \times 40 \text{ mm}^2$ area and a thickness of $200 \mu\text{m}$ will be in operation in August of this year as the focal plane detector of a magnetic spectrometer used for atomic physics experiments. The

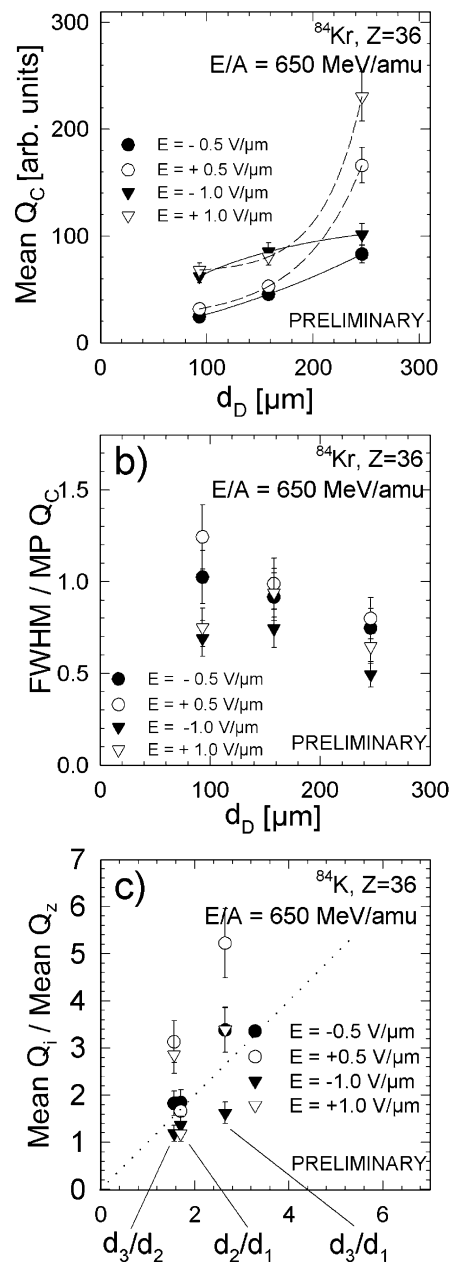


Fig. 9. The mean collected charge Q_C (a) and the pulse-height resolution (b) plotted over the detector thickness. (c) The ratio over the charge collected from two detectors plotted over the corresponding thickness ratio. Q_C increases approximately linear for thin detectors but significantly steeper above $d_D \approx 170 \mu\text{m}$. The broader signals obtained for positive electric field increase stronger. The corresponding resolution FWHM/MP improves with the detector thickness showing best results at highest negative bias.

detector has 32 strips with a pitch of 1.8 mm. Two diamond octagons ($\approx 25 \times 15 \text{ mm}^2$) with eight strips of variable width are implemented as multi-tasking devices providing time-zero and ToF detectors as well as multiplicity and veto devices for the HADES experiment. Various diamond bunch and spill monitors as well as beam intensity and beam profile monitors are

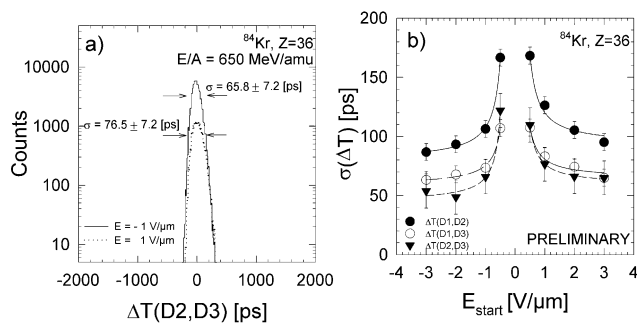


Fig. 10. (a) ^{84}Kr , 650 MeV/amu ToF spectra measured with two detectors with a thickness of 158 μm resp. 246 μm at negative (full line) and positive (dotted line) electric field. No significant difference is observed. (b) The σ -widths of the distributions measured with all three detectors (ΔT_{12} , ΔT_{13} , ΔT_{23}) plotted over the electric field applied. $\sigma(\Delta T)$ improves increasing the bias and saturates above ± 2 V/ μm . Thicker samples are preferable.

already in operation in beam diagnostics applications [8].

The progress in material production [3–5,14] enables the development of CVD-diamond detectors for dosimetry based on current measurements [15]. A large-area position-sensitive carbon dosimeter based on single-particle counting is being developed at GSI [11]. Since the beam intensity needed for the tumor treatment is high ($\approx 5 \times 10^7$ ions/s) the ionisation chambers and MWPCs used at present [16] work at their limits. It should be stressed that besides a much higher reliability required for all detectors used in the tumor treatment the carbon dosimeter operates like a HI beam-profile monitor of high precision.

5. Summary and outlook

The data obtained demonstrate convincingly that CVD diamond detectors used ‘as grown’ are most suitable for HI measurements exploiting single-particle counting and ToF techniques. A new generation broadband electronics is needed to take full advantage of the CVD diamond properties. The time resolution improves with the detector thickness and the electric field applied. The best value achieved at present was $\sigma_i = 29$ ps for two detectors of ‘optical grade’ and a thickness of 100 μm .

An absolute particle monitoring over 10 orders of magnitudes increasing beam intensity becomes possible. This property enables, in addition to beam diagnostic applications, the development of large-area position-sensitive carbon dosimeters suitable for use in tumor therapy. Position-sensitive diamond detectors are suitable for HI tracking devices and for focal plane detectors of magnetic spectrometers. However, the poor pulse-height resolution limits their use in HI experiments requiring energy discrimination of particles. Mi-

crobeam results considered in conjunction with fragmentation data show clearly a dependence on the crystal structure and not on the charge density in the particles track.

The GSI diamond program proceeds testing the suitability of polished CVD diamond ‘detector grade’ for time-zero devices for singly-charged relativistic ionizing particles in experiments with relativistic HIs at the Large Hadron Collider at CERN [17].

Acknowledgements

We would like to thank the FRS crew for the kind support during the Nickel beamtest and the ALICE-TPC group for the excellent collaboration during the Krypton run. It is appropriate to express our gratitude to Bernd Fischer and Michael Schlögl for the microprobe data and to the HADES Collaboration for the ToF spectra of the Start-Veto device provided. Furthermore, extending our thanks to Hans Sann, Yuri Pestov and Rainer Schicker for their comments on this manuscript and for many fruitful discussions on HI diamond detectors.

References

- [1] H. Sann, Position sensitive detectors in heavy ion physics (at GSI), *NIM A* 392 (1997) 433.
- [2] P. Strehl, Ion beam diagnosis, in: B. Wolf (Ed.), *Handbook of Ion Sources*, CRC Press, 1995.
- [3] P. Weilhammer et al., Recent results on CVD diamond radiation sensors, *NIM A* 409 (1998) 264.
- [4] D. Meier et al., Proton irradiation of CVD diamond detectors for high luminosity experiments at the LHC, *NIM A* 426 (1999) 173.
- [5] W. Adam et al., Pulse height distribution and radiation tolerance of CVD-diamond detectors, to be publ. *Proceedings VERTEX*, (1999).
- [6] E. Berdermann, K. Blasche, P. Moritz, H. Stelzer, F. Zeytouni, Diamond detectors for heavy ion measurements, *Proc. XXXVI International Winter Meeting on Nuclear Physics*, Suppl. N. 112, Bormio 1998, Italy.
- [7] D. Tromson, P. Bergonzo, A. Brambilla, C. Mer, F. Foulon, Influence of electrical defects on diamond detection properties, *Diamond Relat. Mater.* 9 (2000) 1091.
- [8] P. Moritz et al., Diamond detectors with subnanosecond time resolution for heavy ion spill diagnostics, *Workshop on Beam Instrumentation* Stanford CA, (1998).
- [9] C. Manfredotti, F. Fizzotti, A. LoGiudice, P. Polesello, E. Vittoni, R. Lu, M. Jaksic, Ion microbeam analysis of CVD diamond, *Diamond Relat. Mater.* 8 (1999) 1597.
- [10] M. Schlögl, B.E. Fischer, Investigation of the detection efficiency of polycrystalline diamond detectors with a heavy ion microprobe, *Proc. of the 5th European Conference on Radiation and its effects on components and systems*, IEEE Cat. No. 99TH8471.

- [11] E. Berdermann, K. Blasche, P. Moritz, H. Stelzer, B. Voss, F. Zeytouni, First applications of CVD-diamond detectors in heavy ion experiments, *Nucl. Phys. B (Proc. Suppl.)* 61B (1998) 399.
- [12] R. Schicker et al., Acceptance and resolution simulation studies for the dielectron spectrometer HADES at GSI, *NIM A* 380 (1996) 586.
- [13] T. Behnke, P. Hüntemeyer, A. Oh, J. Steuerer, A. Wagner, W. Zeuner, The charge collection properties of CVD diamond, *NIM A* 414 (1998) 340.
- [14] DEBID, De Beers Industrial Diamond Division, Charters, UK, England
- [15] C.M. Buttar et al., A study of radiotherapy dosimeters based on diamond grown by chemical vapour deposition, *Diamond Relat. Mater.* 9 (2000) 965.
- [16] B. Voss, H. Junk, H. Stelzer, The monitor system of the therapy project, GSI Scientific Report, (1997).
- [17] M. Petrovici et al., Preliminary results on timing properties of CVD diamond detectors for MIPs, GSI Internal Report, (2000).